Modeling Pharmacokinetics of Doxorubicin in Multiple Myeloma Cells

Alberto Giaretta, Francesco Da Ros, Mario Mazzucato, Morten Gram Pedersen, Roberto Visentin

Abstract— **Doxorubicin (DOXO) is a well-established chemotherapy drug for treatment of different tumors, ranging from breast cancer, melanoma to multiple myeloma (MM). Here, we present a coupled experimental/modeling approach to study DOXO pharmacokinetics in MM cells, investigate its distribution among the extracellular and intracellular compartments during time. Three model candidates are considered and identified. Model selection is performed based on its ability to describe the data both qualitatively and in terms of quantitative indexes. The most parsimonious model consists of a nonlinear structure with a saturation-threshold control of intracellular DOXO efflux by the DOXO bound to the cellular DNA. This structure could explain the hypothesis that MM cells are drug-resistant, likely due to the involvement of P-glycoproteins.**

The proposed model is able to predict the intracellular (free and bound) DOXO and suggests the presence of a saturation-threshold drug-resistant mechanism.

Clinical Relevance— **The model can be used to properly understand and guide further experimental setup, e.g., to investigate multiple myeloma cell variability among different cell lines.**

I. INTRODUCTION

Multiple myeloma (MM) is a hematological neoplasm characterized by abnormal proliferation of plasma cell clones and a tropism for the bone marrow [1], [2]. It represents the third most common blood cancer leading to an abnormal production of paraprotein, organ damage, lytic bone lesions, immunodeficiency. MM showed a global incidence of more than 80,000 cases diagnosed in 2017 and it is expected to increase to over 100,000 by 2027. Currently, the survival rate at 5 years is around the 50% [3]. Despite the increase in survival rate in the last decades, MM remains a treatable but not curable neoplastic disorder. Therefore, patients eligible for autologous transplantation of hematopoietic stem cells are often treated with chemotherapy courses, usually under a multidrug regimen to increase and synergize the therapeutic efficiency [4].

Among chemotherapeutic drugs used in MM treatment, the doxorubicin (DOXO) induces cell death mainly through the inhibition of topoisomerase II [5]. Its employment is well-established and has revealed promising responses in MM treatment [6], [7], [8]. However, cells and tissues can exercise a drug-resistant response that could affect the drug pharmacokinetics (PK). Indeed, DOXO is actively released out of the cell membrane and so loses its efficacy due to the cells expressing the multidrug resistant pump P-glycoprotein (Pgp) [9], [10]. A better understanding of the cell response to the drug is of pivotal importance to properly optimize dosage regimen of current therapeutic protocols. Nowadays, merging mathematical modeling with biological experiments represents an optimal way to achieve such goals, as already done for breast cancer cells treated with DOXO [5]. Indeed, mathematical models can help driving the biological discovery by properly focusing on specific and controlled experiments, as well as being used as simulation tools to predict behaviors under unexplored conditions and optimize/propose novel therapeutic protocols to be tested.

Here we aim at developing a mathematical model of DOXO PK in MM cells. We will propose a suitable model structure among three possible candidates, and we will experimentally and mathematically discuss how DOXO may be subject to an important drug-resistance mechanism in MM cells.

A. Giaretta, M.G. Pedersen, R. Visentin are with the Department of Information Engineering, University of Padova. M.G. Pedersen is also with the Department of Mathematics "Tullio Levi-Civita", University of Padova. F. Da Ros, M. Mazzucato are with the Aviano National Cancer Institute.

Corresponding author: R. Visentin, Department of Information Engineering, University of Padova, via G. Gradenigo 6/B, 35131 Padova, Italy (email: visentin@dei.unipd.it).

II. METHODS

A. Database and protocol

We collected two time courses of 23 samples each measuring extracellular and intracellular DOXO concentration in MM1r cell line.

Two standard curves, for extracellular and intracellular DOXO concentration, respectively, were generated by exploiting the auto-fluorescence property of the drug (Ex: 488nm; Em: 560nm). Serial DOXO dilutions were made in PBS (from 900 nM to 14 nM) and in PBS;FBS 10% (from 3000 nM to 187,5 nM), respectively for intracellular and extracellular concentration. For each time point, 50 µL of PBS or 200 µl of PBS;10% FBS were analyzed in triplicate in microplate of 96 wells with TECAN microplate reader (Ex: 488nm; Em: 560nm) to detect DOXO-associated fluorescence intensity. A linear correlation between fluorescence intensity and DOXO concentration was achieved for both solutions (Fig.1).

MM1r cell line was used to study DOXO cellular uptake and release. Two days prior the analysis, cells were plated in RPMI 1640;10% FBS; Pen/Strep; in microplate of 96 wells at a density of 10^5/well to permit a slight adhesion. For each time point, cells were plated in triplicate. After two days, the medium was removed from all wells, cells were washed in PBS and, at time t=0 hr treated with 1 µM DOXO in PBS, 10%FBS, 200 µL/well. To observe DOXO uptake, from $t = 0$ to $t = 1$ hrs, every 5 min, 200 µL of PBS;
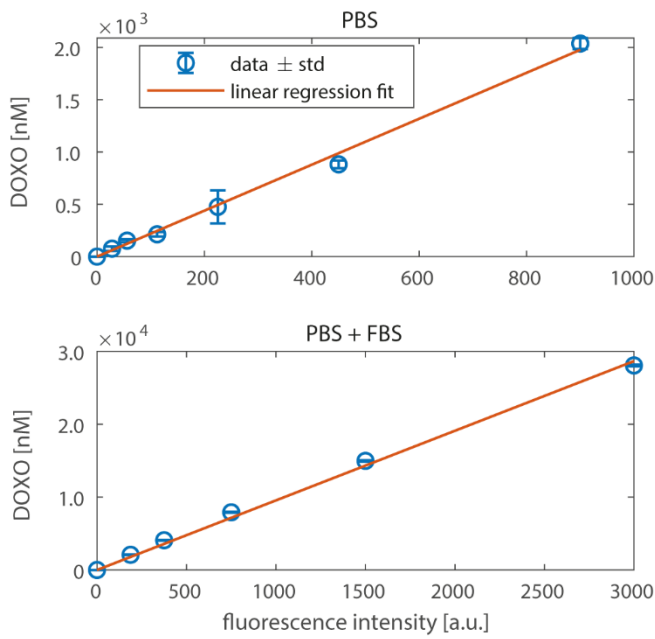
Fig.1 Linear regression between fluorescence intensity and DOXO concentration in intracellular (PBD, *upper panel*) and extracellular (PBS+FBS, *lower panel*) compartments.

10%FBS+DOXO were moved to an empty well, cells were washed once in PBS and maintained in 50 μL of fresh PBS. The extracellular (200 μl of PBS; 10%FBS) and intracellular (cells in 50 μl of PBS) DOXO-associated fluorescence intensities were then acquired with TECAN microplate
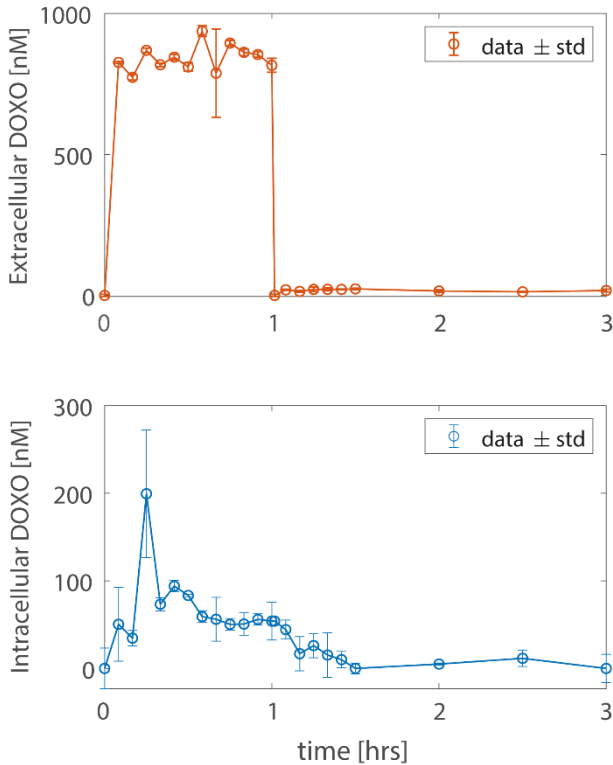

Fig.2 DOXO concentration time courses. Extracellular (*upper panel*) and intracellular (*lower panel*) DOXO concentrations are reported in blue and orange, respectively. Concentrations are expressed in [nM].

reader. To observe DOXO release by MM1r cells, at $t = 1$ hr DOXO was removed, cells were washed with PBS, and 200 μl of fresh PBS; 10% FBS were added. Every 5 minutes from $t = 1$ to $t = 1.5$ hrs and at $t = 2, 2.5, 3$ hrs, extracellular and intracellular DOXO fluorescence intensity was collected with the same approach used for the uptake study. For each time point, both extracellular and intracellular DOXO concentrations were obtained by fluorescence intensity using the respective standard curves described above (Fig. 2). To note, extracellular and intracellular concentrations at $t = 0.66$ hr and $t = 0.25$ hr, respectively, showed a high variability in the triplicate measurements (standard deviations >400% of the average ones), likely due to a failure in the experimental procedure. Therefore, these samples were excluded from the following analysis.
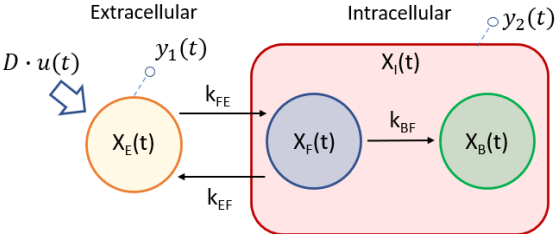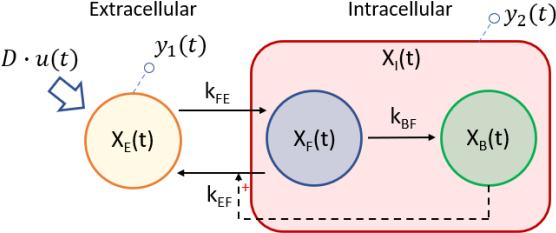
B. Modeling DOXO Pharmacokinetics

We compare three model structures describing DOXO pharmacokinetics (PK), as summarized in Table I.

A first simple structure (Model 1) is considered based on a recent work describing DOXO PK in breast cancer cell lines [5]. It is a linear three-compartment model describing DOXO concentrations in the extracellular (X_E) and intracellular compartments (X_I). This latter is composed by two compartments representing free intracellular DOXO (X_F) and DOXO bound to the DNA (X_B) inside the cell nucleus, where $X_I(t) = X_F(t) + X_B(t)$. The input is delivered as a DOXO dose impulse in the extracellular compartment. No drug degradation is taken into account, since its half-life (~17 hrs [11]) is much higher than the duration of the experiment (i.e., 3 hrs) and because the experiments are performed under a controlled environment. k_{FE} and k_{EF} are the rate constants describing DOXO transit from extracellular to free intracellular compartment and vice versa, respectively. k_{BF} is the rate constant describing binding of free intracellular DOXO to DNA, which is assumed to be irreversible. V_E is the volume of the extracellular compartment, which was set to 200 μL, i.e., the volume of media in each well. V_I is the volume of the intracellular compartment which is calculated by multiplying the number of cells seeded ($\sim 10^5$) by an estimate of the single cell volume, considering the cell as a sphere with diameter equal to 10 μm.

Model 2 and 3 are derived from Model 1 with an extra control on k_{EF} rate constant from the intracellular bound DOXO ($X_B(t)$) compartment. In this scenario $k_{EF}(X_B(t))$ is modeled in terms of a Hill function as reported in Table I (fourth equation, third row). The Hill function typically describes threshold and saturation phenomenon [12] and is defined by three parameters: k_{th} denotes the $X_B(t)$ concentration at which $k_{EF}(X_B(t))$ is half its maximum value V_{max}. The Hill coefficient q determines the sharpness of the transition. Note that for $q = 1$ the Hill relation collapses to the Michaelis-Menten form, capable to describe only pure saturation controls [12]. In particular, Models 2 and 3 are characterized to have a Michaelis-Menten ($q = 1$) and a Hill function ($q = 2$) controls on $k_{EF}(X_B(t))$, respectively.

For all the three model structures, the input function is $I(t) = D \cdot u(t)$, where $D = 1000$ nM is the known DOXO dose concentration and $u(t) = \delta(t)$ is a Dirac delta.

TABLE I.   COMPARTMENT MODELS OF DOXO PK

Model structure	Model equations	Number of parameters
	$\begin{cases} \dot{X}_E(t) = k_{EF}\dfrac{V_I}{V_E}X_F(t) - k_{FE}X_E(t) + I(t) & X_E(0) = 0 \\[2mm] \dot{X}_F(t) = k_{FE}\dfrac{V_E}{V_I}X_E(t) - k_{EF}X_F(t) - k_{BF}X_F(t) & X_F(0) = 0 \\[2mm] \dot{X}_B(t) = k_{BF}X_F(t) & X_B(0) = 0 \end{cases}$	3
	$\begin{cases} \dot{X}_E(t) = k_{EF}(X_B(t))\dfrac{V_I}{V_E}X_F(t) - k_{FE}X_E(t) + I(t) & X_E(0) = 0 \\[2mm] \dot{X}_F(t) = k_{FE}\dfrac{V_E}{V_I}X_E(t) - k_{EF}(X_B(t))X_F(t) - k_{BF}X_F(t) & X_F(0) = 0 \\[2mm] \dot{X}_B(t) = k_{BF}X_F(t) & X_B(0) = 0 \end{cases}$ $$k_{EF}(X_B(t)) = \frac{V_{max}X_B(t)^q}{k_{th}^q + X_B(t)^q}, \quad q \in \{1,2\}$$	5

Model 1 is described in [10], while Model 2 and 3 are its proposed refinements. Signals u, y_1 and y_2 represent the DOXO input and extra-/intra-cellular DOXO concentration, respectively. Intracellular space, accounting for both free and bound DOXO compartments, is included in the red area.

C. Model identification

For $t = 0,...,3$ hrs, the measurement vector is:

$$y(t) = [y_1(t)\; y_2(t)] = [X_E(t)\; X_I(t)] \qquad (1)$$

in other words, the extracellular and the total intracellular compartments are observable.

The measurement model we have chosen to perform the parameter identification is the following:

$$y_2(t) = \hat{X}_I(t; \boldsymbol{\theta}_i) + e(t), \quad i = 1,2,3; \; t = t_1,\dots,t_N \qquad (2)$$

where $\hat{X}_I(t; \boldsymbol{\theta}_i)$ is the i-th model prediction for the total intracellular compartment and $y_2(t)$ is the system output related to the measurements of the free compartment corrupted by a zero-mean white Gaussian noise $e(t)$ of known variance $\sigma^2(t)$, i.e., $e(t)\sim\mathcal{N}(0, \sigma^2(t))$. The variance of the measurement error was calculated at each time point by exploiting the time series in triplicate.

$\boldsymbol{\theta}_i$ is the parameter vector for the three investigated model structures. In particular, $\boldsymbol{\theta}_1 = [k_{FE}\; k_{EF}\; k_{BF}]$ for the Model 1 and $\boldsymbol{\theta}_{2/3} = [k_{FE}\; k_{EF}\; k_{BF}\; V_{max}\; k_{th}]$ for the Models 2 and 3. q is fixed for Models 2 and 3, as described in section B.

The parameter vectors $\boldsymbol{\theta}_i$ where estimated by means of nonlinear weighted least squares (WLS) implemented in MATLAB 2020b (Natick , MA) in order to fit the time courses of the total intracellular compartment $X_I(t)$. Therefore, we can write:

$$\hat{\boldsymbol{\theta}}_i^{WLS} = \arg\min_{\boldsymbol{\theta}_i} WRSS(\boldsymbol{\theta}_i)$$
$$= \arg\min_{\boldsymbol{\theta}_i}\left\|y_2 - \hat{X}_I(\hat{X}_F,\hat{X}_B,X_E; \boldsymbol{\theta}_i)\right\|_{\Sigma_e}^2$$
$$s.t. \; X_E(t) = y_2(t), \; t = t_1,\dots,t_N \qquad (3)$$

where $\hat{\boldsymbol{\theta}}_i^{WLS}$ is the parameter vector estimate and $WRSS(\boldsymbol{\theta}_i)$ is the weighted residual sum of squares that can be written as

the squared norm of the residuals, $\boldsymbol{res} = \boldsymbol{y_2} - \hat{X}_I(\hat{X}_F,\hat{X}_B,X_E; \boldsymbol{\theta}_i)$, weighted on the covariance matrix $\Sigma_e = Cov(\boldsymbol{e})$ of the measurement error vector $\boldsymbol{e} = [e(t_1)\cdots e(t_N)]$. $\hat{X}_I(\hat{X}_F,\hat{X}_B,X_E; \boldsymbol{\theta}_i)$ is the prediction vector of the model, for the total intracellular compartment, obtained by solving the system of differential equations in Table I with parameter vector $\boldsymbol{\theta}_i$. The condition "$s.t.\; X_E(t) = y_2(t)$, $t = t_1,\dots,t_N$" implies that the extracellular compartment was treated as an experimentally controlled input function and was not fit by the model.

We point out that initial parameter values were fixed to parameters found for similar model structures in breast cancer cell lines [5].

As detailed in section II.A, the intracellular measurement at time $t = 0.25$ hrs was assumed to be an outlier and hence its contribution was not considered during the parameter estimation.

D. Model validation and selection

The best model structure was selected among the three candidates based on different criteria. Firstly, for each model the Akaike information criteria (AIC) [12] has been computed as:

$$AIC_i = WRSS(\theta_i) + 2P_i, \; i = 1,2,3 \qquad (4)$$

where AIC_i and P_i are the AIC and number of parameters of the i-th model structure, respectively.

Besides AIC, we also made sure to obtain consistent results in terms of WRSS and of a posteriori identifiability assessed in terms of precision of parameter estimates (coefficient of variation (CV) below 100 %), as well as by looking at the average CV for the estimated parameters. CV is obtained from the inverse of the Fisher information matrix [12]. Randomness of the residuals was assessed by the Runs
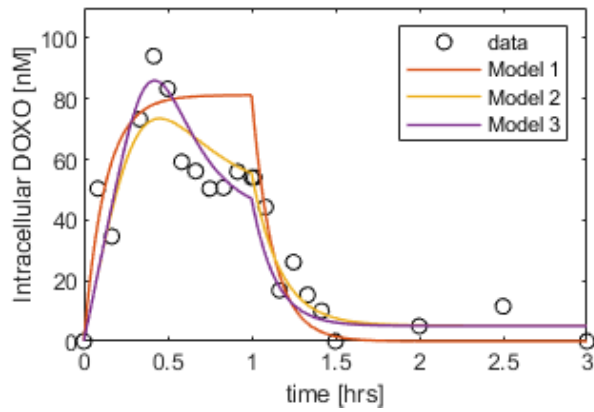
Fig.3 Intracellular DOXO data (black dots) against prediction obtained with Model 1 (orange line) Model 2 (yellow line) and Model 3 (purple line), respectively.

TABLE II. MODEL PARAMETER ESTIMATES

Model	k_{FE} $[hr^{-1}]$	k_{BF} $[hr^{-1}]$	k_{EF} $[hr^{-1}]$	k_{th} $[nM]$	V_{max} $[hr^{-1}]$
1	1.77e-04 (20%)	0.05 (31%)	8.48 (21%)	-	-
2	7.76e-05 (12%)	0.08 (26%)	-	18.01 (167%)	38.21 (133%)
3	7.05e-05 (10%)	0.08 (27%)	-	2.28 (36%)	8.66 (17%)

Precision of parameter estimates is reported between parenthesis as coefficient of variation (CV, defined as the ratio between the standard deviation of the estimated parameter and the parameter value).

test for all the three model structures [12]. Moreover, we made sure to have estimated parameter values consistent with a reasonable biological range, inferred from the current literature [12].

III. RESULTS

A. Model fit and parameter estimation

Model 1: The model was not capable to predict the intracellular DOXO data, apart from the first transient phase, as shown in Fig.3. In particular, the model completely lacks capacity to describe the first decreasing phase occurring between 0.5 and 1 hrs. This was probably due to the model structure not entirely suitable to describe the observed phenomena. On the other hand, model parameters were estimated with good precision, with all CV lower than 40% (Table II).

Model 2: Compared to Model 1, Model 2 was able to better predict the data, particularly improving the performance during the decreasing phase after the first 0.5 hrs of DOXO treatment (Fig. 3). Precision of parameter estimates was not satisfactory, specifically CV was higher than 100% for both V_{max} and k_{th} estimates (Table II). This is probably due to the need for a mixed effect between threshold and saturation acting on k_{EF}, while a Michaelis-Menten control accounts only for the saturation effect.

Model 3: The model was able to predict the data qualitatively and quantitatively. It was capable to well describe the decreasing phase after the first 0.5 hrs of DOXO treatment, as well as the final decreasing phase, after DOXO withdrawal (Fig. 3). Model parameters were estimated with good precision, with all CV<100% (Table II). This suggests

TABLE III. MODEL COMPARISON

Model	WRSS	$\overline{CV}$ %	Plausibility of Model Parameters*	AIC
1	82.52	23.94%	Yes	88.52
2	22.17	84.48%	Yes	30.17
3	17.88	22.57%	Yes	25.88

*Plausibility of model parameters assessed in terms of the biological range inferred from literature.

that the saturation-threshold mechanism introduced by a Hill-based control on k_{EF} is well suited to properly describe the observed phenomenon. Parameter estimates were biologically plausible, as well (Table III).

B. Model selection

Model comparison is summarized in Table III. Model 3 provided the best parameter estimate precision (on average, $\overline{CV} = 23.94\%$ and $\overline{CV} = 22.57\%$, for Model 1 and 3, respectively). However, Model 3 showed the best qualitative coherence with the data, as shown in Fig. 3, and the lowest AIC and WRSS indexes. Therefore, Model 3 was selected as the most parsimonious.

In Fig. 4 we show the Model 3 predictions of the three state variables. We can observe how the model predicts a very low amount of DOXO bound to the cell DNA with slow dynamics, and free intracellular DOXO results very close to the total intracellular DOXO concentration.

IV. CONCLUSION

Doxorubicin (DOXO) uptake and release by multiple myeloma (MM) cell line was performed taking advantage of autoflourescent property of the drug. The obtained dataset was used to propose a mathematical model of DOXO PK in MM cells capable of describing the DOXO drug distribution in the extracellular and intracellular compartments. The intracellular compartment was considered to be composed of two further compartments related to free and bound DOXO. The mathematical model structure was selected among three possible candidates. The first model structure (Model 1) was chosen from a recent linear model of DOXO PK in breast cancer cell lines [5]. However, in our data we notice a clear decrease of intracellular DOXO after the first 0.5 hrs of treatment, which Model 1 was unable to properly predict.
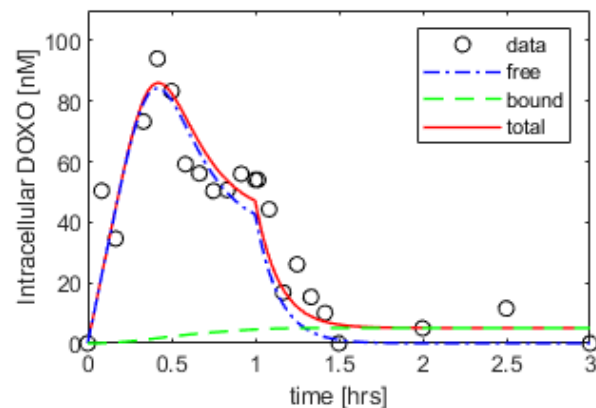

Fig.4 Intracellular DOXO data (black dots) against Model 3 prediction (red line), with its free (blue dashed-dotted line) and bound (green dashed line) contributions.

This drug decrease might be attributable to a drug resistance mechanism activated after a proper delay. It is well known that DOXO is a strong inducer of cell death but it is ineffective in P-glycoprotein (Pgp)-expressing cells that can favor the DOXO efflux into the extracellular compartment, hence providing a drug-resistance mechanism [9], [10]. It could be possible that the activation of the Pgp trafficking from intracellular Pgp buffer towards the cell membrane [9], [10] is responsible for the drug-resistant mechanism, as well as the related delay. For this reason, we have introduced other two model structures capable of accounting for the DOXO decreasing phenomenon. Since the Pgp activity was not explicitly measured in this work, we phenomenologically modeled the efflux rate control (k_{EF}) through the DOXO bound compartment through a Michaelis-Menten control (Model 2) or a Hill-based control (Model 3).

Despite a similar good performance in terms of parameter estimate precision between Models 1 and 3, Model 3 resulted to be the most parsimonious model in terms of WRSS and AIC index. This result suggests that in MM the DOXO drug resistance may be mediated by a threshold/saturation control of the DOXO bound to the DNA. In a more mechanistic scenario, it could be plausible to assume that the DOXO drug resistance mechanism in MM cells is a threshold/saturation control related to the Pgp cellular trafficking activated by the presence of intracellular DOXO drug.

Finally, the model well described the intracellular DOXO compartment and was used to predict the DOXO bound inside the cell nucleus. This latter was predicted to have a very low concentration and slow dynamics, suggesting that only a little fraction of the DOXO drug reaches the nucleus hence inducing the cell death. This is another interesting result and suggests that k_{BF} rate constant could be an important parameter to tune in order to increase the drug efficiency. However, these results call for further experiments to prove that only a small DOXO fraction binds the cell DNA, as well as to prove that Pgp trafficking is responsible for the drug-resistance behavior observed in the experiments. This will also allow to properly assess model robustness. Indeed, here we used a single set of experimental data, precluding the evaluation of possible model overfitting.

This work represents a first starting point for a deeper investigation of DOXO PK in order to mechanistically understand the drug resistance features of MM cell lines. Further important questions will regard the potential dose-dependent DOXO PK, as well as investigating the DOXO PK variability among different MM cell lines. As far as we know, this is the first work modeling the DOXO PK in MM cells, as well as showing a potential evident drug-resistance mechanism.

REFERENCES

[1] B. Sirohi and R. Powles, "Multiple myeloma," vol. 363, pp. 875–887, 2004.

[2] R. Eslick, "Multiple myeloma : from diagnosis to treatment," vol. 42, no. 10, pp. 684–688, 2013.

[3] D. Kazandjian and L. M. Branch, "HHS Public Access," vol. 43, no. 6, pp. 676–681, 2017, doi: 10.1053/j.seminoncol.2016.11.004.Multiple.

[4] H. N. Abramson, "The Multiple Myeloma Drug Pipeline—2018: A Review of Small Molecules and Their Therapeutic Targets," *Clin. Lymphoma, Myeloma Leuk.*, vol. 18, no. 9, pp. 611–627, 2018, doi: 10.1016/j.clml.2018.06.015.

[5] M. T. Mckenna *et al.*, "Modeling Approach for the Study of Doxorubicin Treatment in Triple Negative Breast Cancer," *Sci. Rep.*, no. June, pp. 1–14, 2017, doi: 10.1038/s41598-017-05902-z.

[6] P. S. Becker *et al.*, "A phase 2 study of bortezomib, cyclophosphamide, pegylated liposomal doxorubicin and dexamethasone for newly diagnosed multiple myeloma," *Blood Cancer J.*, vol. 6, p. e422, 2016, doi: 10.1038/bcj.2016.31.

[7] A. G. Mittenberg *et al.*, "Combined treatment of human multiple myeloma cells with bortezomib and doxorubicin alters the interactome of 20S proteasomes," *Cell Cycle*, vol. 17, no. 14, pp. 1745–1756, 2018, doi: 10.1080/15384101.2018.1496742.

[8] M. A. Schroeder *et al.*, "A phase I/II trial of carfilzomib, pegylated liposomal doxorubicin, and dexamethasone for the treatment of relapsed/refractory multiple myeloma," *Clin. Cancer Res.*, vol. 25, no. 13, pp. 3776–3783, 2019, doi: 10.1158/1078-0432.CCR-18-1909.

[9] M. E. Tome *et al.*, "P-glycoprotein traffics from the nucleus to the plasma membrane in rat brain endothelium during inflammatory pain," 2016, doi: 10.1177/0271678X16661728.

[10] M. T. Mckenna, J. A. Weis, V. Quaranta, and T. E. Yankeelov, "Leveraging Mathematical Modeling to Quantify Pharmacokinetic and Pharmacodynamic Pathways : Equivalent Dose Metric," vol. 10, no. May, pp. 1–16, 2019, doi: 10.3389/fphys.2019.00616.

[11] A. Rahman and M. Harris, "Comparative pharmacokinetics of free doxorubicin and doxorubicin (DX) entrapped in cardiolipin liposomes," *Proc. Am. Assoc. Cancer Res.*, vol. VOL. 26, no. May, pp. 2295–2299, 1985.

[12] C. Cobelli and E. Carson, *Introduction to Modeling in Physiology and Medicine*. Academic Press, 2008.